AB-MTEDeep Classifier Trained with AAGAN for the Identification and Classification of Alopecia Areata

Chinnaiyan Saraswathi
Department of Computer and Information Science, Faculty of Science, Annamalai University, India
saraswathichinnaiyan@gmail.com (corresponding author)

Balasubramanian Pushpa
Department of Computer and Information Science, Faculty of Science, Annamalai University, India
pushpasidhu@gmail.com

Received: 15 March 2023 | Revised: 7 April 2023 | Accepted: 17 April 2023

 DOI: https://doi.org/10.48084/etasr.5852

ABSTRACT

Artificial Intelligence (AI) is widely used in dermatology to analyze trichoscopy imaging and assess Alopecia Areata (AA) and scalp hair problems. From this viewpoint, the Attention-based Balanced Multi-Tasking Ensembling Deep (AB-MTEDeep) network was developed, which combined the Faster Residual Convolutional Neural Network (FRCNN) and Long Short-Term Memory (LSTM) network with cross residual learning to classify scalp images into different AA classes. This article presents a new data augmentation model called AA-Generative Adversarial Network (AA-GAN) to produce a huge number of images from a set of input images. The structure of AA-GAN and its loss functions are comparable to those of standard GAN, which encompasses a generator and a discriminator network. To generate high-quality AA structure-based images, the generator was trained to extract the 2D orientation and confidence maps along with the bust depth map from real hair and scalp images. The discriminator was also used to separate real from generated images, which were provided as feedback to the generator to create synthetic images that are extremely close to the real input images. The created images were used to train the AB-MTEDeep model for AA classification. Finally, the experimental results exhibited that the AA-GAN-AB-MTEDeep achieved 96.94% accuracy.

Keywords-artificial intelligence; Alopecia Areata; deep learning; data augmentation; GAN

I. INTRODUCTION

Hair loss or scalp problems are usually caused by stressful situations [1]. Nowadays, many individuals have scalp illnesses like psoriasis, baldness, etc., as a result of several issues, including bad daily routines, unequal weight growth, extreme weariness, and dangerous environments [2-3]. The function of iron and nutritional supplements in the diagnosis of baldness was examined in [4]. The most common kind of hair loss, known as Alopecia Areata (AA), affects up to 70% of men and 40% of women [5]. Problems with scalp hair can be influenced by internal factors such as endocrine, hereditary, illness, and others. Many cases of psoriasis, cellulitis, and associated signs and symptoms were reported in France [6]. According to many studies, psoriasis affects about 18% of children in the US and Australia. As a result, both adults and children might experience scalp problems. Therefore, it is important to know how to properly manage the scalp and prevent diseases linked to baldness. Recently, specialized therapies have emerged to address severe scalp disorders [7].

The state of a patient's scalp is assessed manually in the most frequently used analytical processes for treating baldness. However, these manual diagnostic examinations can provide a wide range of findings and raise questions about the diagnosis and health of the scalp since they depend on the skills of the physiotherapist [8]. A substantial amount of effort and money have been invested in continuously developing physiotherapy skill sets [9]. Another significant problem is the variations in how scalp hair microscope pictures should be interpreted, even among licensed and experienced physiotherapists. Such discrepancies in medical interventions might be attributed to ignorance [10].

ScalpEye [11] is a deep learning-based scalp identification system developed to overcome these issues. A minority of people experience a patch of hair loss, while other people report more severe or uncommon issues [12]. In recent years, numerous scalp and dermoscopic images have been employed in recognizing and diagnosing AA. Trichoscopy and biopsies are frequently necessary to identify and diagnose AA as the reason for hair loss [13]. One of the main problems with these diagnostics is the number of tests required for a reliable

diagnosis. Additional research on AA diagnosis and detection using AI methods, such as Support Vector Machine (SVM), Artificial Neural Networks (ANNs), Convolutional Neural Networks (CNNs), and others, is highly encouraged [14]. According to this perspective, a correct diagnosis requires the simultaneous recognition of AA and scalp condition. To achieve this, an Ensemble Parameter Optimized LSTM-based Pre-learned DL (EPOLSTM-PDL) model, which combined LSTM and pre-trained CNNs such as AlexNet, ResNet, and InceptionNet was proposed in [15]. The pre-trained CNNs were used to capture the deep features from the hair and scalp images, which were learned by the LSTM network. The LSTM's hyperparameters were chosen by the Battle Royale Optimization (BRO) algorithm. But, if the network depth is increased, degradation problem occurrs causing overfitting. Therefore, the Attention-based Balanced Multi-Tasking Ensembling Deep (AB-MTEDeep) model was developed, which adopted cross-residual learning in the LSTM with FRCNN to improve efficiency [16]. However, the robustness and generalization ability of the deep learning models largely depends on the amount of data available in the training phase. According to this, it is essential to have an adequate number of images for efficient training.

This paper proposes a new data augmentation model called AA-GAN to generate a large number of images from given input images. The design and loss functions of this AA-GAN are analogous to tose of the standard GAN, which comprises both a generator and a discriminator. For real hair and scalp images, the generator was trained to reconstruct high-quality AA structure-based images according to the extraction of the 2D orientation and confidence maps, along with a bust depth map. Moreover, the discriminator was used to distinguish real and generated images which were given as feedback to the generator to generate synthetic images very closer to the real input images. Furthermore, the created images were used to train the AB-MTEDeep model, which was used to classify the test images into different AA classes. Thus, the AA-GAN can increase the number of training images for more effective classification of AA conditions.

II. RELATED WORKS

In [17], a novel data augmentation method was proposed, called Random Image Cropping and Patching (RICAP), which randomly cropped and patched an input image to generate a new training image for CNN. Also, the class labels of the actual images were mixed to gain the benefit of soft labels, However, it needed to choose the appropriate hyperparameters for effective performance. In [18], the presented StyleGAN was used to generate high-quality nodule images fed to the Transfer-ResNet50 to classify tumors, but it needed further enhancement in the diversity of the created images. In [19], an Enhanced Framework of GANs (EF-GANs) was designed for VGG16, integrating geometric transformation schemes and GANs for image augmentation. In [20], the Self-attention Progressive Growing of GANs (SPGGANs) was proposed to create more fine-grained nodule scans by fusing details from all feature positions, and the Two-Timescale Update Rule (TTUR) was applied to enhance the model's robustness. In [21], the Zero Shot Augmentation Learning (ZSAL) framework was presented for health signal processing. Initially, the contour of a lesion was recognized by a skilled physician, and a background image without a lesion was chosen. In [22], a novel Inception-Augmentation GAN (IAGAN) was proposed to create new X-ray scans that could help detect pneumonia and COVID-19. In [23], a generic adversarial data augmentation model called AdvChain was proposed to enhance the diversity and efficiency of learning data for medical image segmentation. In [24], a new model called XtremeAugment was developed for labeling and augmenting images, using Hardware Dataset Augmentation (HAD) and Object-Based Augmentation (OBA). The HAD was used to enable users to acquire more data, whereas the OBA was used to increase the training data variability and maintain the distribution of the augmented images being similar to the actual data. But, this approach needed annotated images for efficient training and was not effective with very limited images.

III. PROPOSED METHODOLOGY

Figure 1 presents an overall schematic of the proposed AA-GAN.

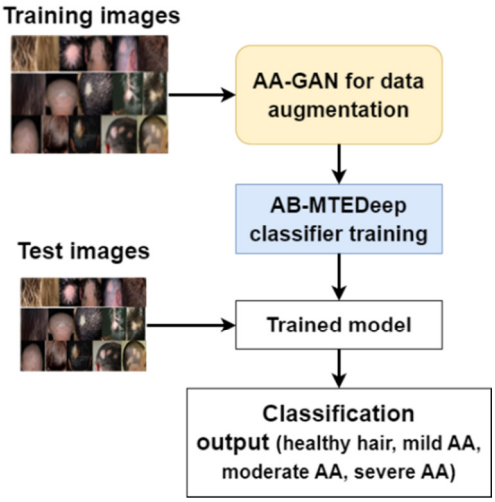

Fig. 1. Schematic representation of the proposed study.

A. Image Collection

This system used the following 2 openly accessible datasets for analysis:

- Figaro1k dataset, which is a public dataset enclosing 1050 hair photos, evenly allocated into distinct types like straight, wavy, and curly [25].
- Dermnet dataset, which is a public dataset accessible on Dermnet [26], enclosing 23 types of dermatological illnesses with AA. Overall, 108 photos were obtained for 3 distinct AA types: mild, moderate, and severe.

Figure 2 shows a few examples of scalp hair photos in multiple labels from the given databases.

Fig. 2. Scalp hair photo examples of the Dermnet and Figaro1k databases.

B. Data Preparation for AA-GAN

A fused model space was initially defined to create the training dataset. At first, a bounding box was defined as the boundary of the model space, where the ground-truth 3D hair orientation volume was generated and 2D hair orientation and confidence maps were extracted.

Bounding box: The model space was constrained by a bounding box defined by the bust model and each hair model of the dataset, excluding a few extremely long hairs. After that, a 3D volume with a resolution of 128×128×128 was split in the bounding box.

2D capture: To obtain 2D information maps X under the defined model space, the center of the image plane matched with the center of the bounding box. The 2D image was obtained by orthogonal projection with a scale of 1024/H. So, the dimension of the obtained image was 1024×1024.

After that, the dataset was doubled by flipping all models, and constrained hairstyles such as braids and bounds were eliminated. In the considered dataset, 1050 hairstyles were available, which differ from straight to curly and short to long. The hair around the center of the bounding box was rotated arbitrarily. The rotation ranged from -15° to 15° for the X-axis, -30° to 30° for the Y-axis, and -20° to 20° for the Z-axis. As each dataset model was prepared by polygon strips, they were transformed to a dense 3D orientation volume viewed as the ground truth Y and grew strands later. Afterward, the hair strands were rendered to the 2D image at the camera view pose. Additionally, the bust model was considered a condition for AA-GAN because hair grows on the scalp and circulates the body. The bust depth map was determined by ray tracing, pixel by pixel, to obtain the distance from the bust to the camera, and the distance was split by D to vary the value within [0,1]. Finally, the network input X was created using the 2D orientation map, confidence map, and bust depth map. Every 2D map was valued within [0,1] and the 3D and 2D orientation vectors were encoded in color space. For all dataset models, N pairs of X and Y were determined as training data.

C. Design and Training of Alopecia Areata – Generative Adversarial Network

With the 2D maps and the bust depth map captured from the input image, AA-GAN aimed to create a 3D orientation volume encoding both occupancy and orientation data to guide the AA scalp hair image augmentation. The input of the network was a 2D tensor X with a dimension of 1024×1024, consisting of 4 feature channels, which were acquired in the unified model space: hair orientation map (the 2D direction vector XY encoded as the color of RG), confidence map (the confidence value as the color of gray), and bust depth map (the depth value as the color of gray). The output was a 3D tensor Y of dimension 128×128×96, where the hair orientation vectors were encoded in RGB.

1) Loss Functions

The GAN is trained by the game-theory approach between the generator and discriminator. The aim was to train the generator G(X) that maps the input 2D tensor to a required output 3D tensor $\tilde{Y}$: $\tilde{Y} = G(X)$. Meanwhile, the discriminator maximizes the Wasserstein-1 distance between the generator distribution of $G(X)$ and the target distribution of Y with a conditional latent projection $P(X)$. The objective of the discriminator is to reduce the loss as:

$$L_D = \mathbb{E}\left[D\left(\tilde{Y}, P(X)\right)\right] - \mathbb{E}\left[D(Y, P(X))\right] + \lambda \mathbb{E}\left[\left(\left\|\nabla_{\tilde{Y}} D\left(\tilde{Y}, P(X)\right)\right\|_2 - 1\right)^2\right] \quad (1)$$

where the third term is the gradient penalty for random samples $\tilde{Y}$, that $\tilde{Y} \leftarrow \epsilon Y + (1-\epsilon)Y$, and ϵ is a random number in [0,1]. The coefficient λ was set to 10, $P(\cdot)$ is the CNN to map 2D tensor X into a 3D latent space to be combined with Y or $\tilde{Y}$, and the parameters in $P(\cdot)$ are trained along with those of D. Similarly, the loss function for a generator is described by:

$$L_D = -\mathbb{E}\left[D\left(\tilde{Y}, P(X)\right)\right] \quad (2)$$

This function does not perform well to fine-tune the generator, because the distribution variance between the actual and the counterfeit cannot be simply calculated by the plus or minus signs. According to the fact that only selected layers of pre-learned networks are used as feature representations to transfer texture style from a source to the target image, the losses of style and content were adopted, where the features were defined in the domains of selected discriminator layers. So, the objective of fine-tuning the generator was to reduce the loss:

$$L_G^* = \alpha L_{content} + \beta L_{style} \quad = \alpha \sum_l L_{content}^l + \beta \sum_l L_{style}^l \quad (3)$$

where α and β are the weighting factors. The content loss was taken as the square-error loss between feature representations:

$$L_{content}^l = \frac{1}{2} \sum_{ik} \left[f_{ik}^l\left(Y, P(X)\right) - f_{ik}^l\left(\tilde{Y}, P(X)\right)\right]^2 \quad (4)$$

where l is a selected layer, i is the i^{th} feature map, k is the index in the feature tensor, and f describes the discriminator features. The style loss is defined by the mean-squared distance between the Gram matrices, where all elements were computed by the inner product between the vectorized feature maps i and j: $A_{ij}^{l} = \sum_k f_{ik}^{l} f_{jk}^{l}$. The objective was:

$$L_{style}^{l} = \frac{1}{4N_l^2 M_l^2} \sum_{ij} \left[A_{ij}^{l}(Y, P(X)) - A_{ij}^{l}\left(\tilde{Y}, P(X)\right) \right]^2 \quad (5)$$

where N_l was the number of feature maps and M_l was the size of feature tensors.

2) Design

Table I shows the generator and discriminator structures. The following notations were used to define the structure of the proposed AA-GAN: The input and output data fo the processing units are *in*(*resolution*, *feature channels*) and *out*(*resolution*, *feature channels*), *C*(*input channels*, *output channels*, *stride*) is the convolutional layer with a ReLU activation, ϖ is the dimensional expansion layer, and ζ is the fully connected node. Also, + was used as the element-wise addition in the residual blocks created by *C*, and *I* was the input tensor of the current layer. For each 2D convolutional layer C_2, the filter size was 5 and 3 for each 3D convolutional layer C_3. The processing units for *X*-, *Y*-, and *Z*-info contain similar strategies.

TABLE I. GENERATOR AND DISCRIMINATOR STRUCTURE

Generator		$in(1024 \times 1024,4) \Leftarrow X$ $C_2(4,16,2) + [C_2(4,8,2), C_2(8,16,1)]$ $C_2(16,64,2) + [C_2(16,32,2), C_2(32,64,1)]$ $C_2(64,256,1) +$ $[C_2(64,128,2), C_2(128,256,1)]$ $I + [C_2(256,256,1), C_2(256,256,1)]$ $out(128 \times 128,256)$
***X*-, *Y*-, *Z*-blocks**		$in(128 \times 128,256)$ $I + [C_2(256,256,1), C_2(256,256,1)]$ $I + [C_2(256,256,1), C_2(256,256,1)]$ $C_2(256,128,1)$ $C_2(128,96,1)$ ϖ $out(128 \times 128 \times 96,1)$
Concatenation of the *out* from *X*-, *Y*-, *Z*-blocks		$in(128 \times 128 \times 96,3)$ $I + [C_3(3,3,1), C_3(3,3,1)]$ $I + [C_3(3,3,1), C_3(3,3,1)]$ $out(128 \times 128 \times 96,3) \Rightarrow \tilde{Y}$
Discriminator	***P*(·) block**	$in(1024 \times 1024,4) \Leftarrow X$ $C_2(4,32,2)$ $C_2(32,64,2)$ $C_2(128,96,1)$ ϖ $out(128 \times 128 \times 96,1)$
	Concatenation of $\tilde{Y}/Y$ with $P(X)$	$in(128 \times 128 \times 96,4)$ $C_3(4,32,2)$ $C_3(32,64,2)$ $C_3(64,128,2)$ $C_3(126,256,2)$ $C_3(256,512,2)$ ζ

Generator: The initial block with input *X*, consisting of 4 residual network elements-wisely adding activation from the previous layer to successive layers to obtain a residual correction from high- to low-level data, downsamples feature maps to a latent code from 1024×1024 to 128×128, along with the number of features increasing from 4 to 256. After that, *X*-, *Y*-, and *Z*-blocks independently encode the latent code to features with 96 channels and the resolution along the *Z*-axis in the resulting volume. As well, ϖ transforms the series of 2D features into a single channel of 3D features. Then, the output from *X*-, *Y*-, and *Z*-blocks are concatenated and given to the following 3D residual convolutional networks.

Discriminator: Considering the correspondence between the 2D input *X* and the 3D desired output $\tilde{Y}/Y$, the latter was concatenated with $P(X)$, a feature map encoding *X* to a 3D latent space with a similar resolution as $\tilde{Y}/Y$. Subsequently, the concatenated 3D feature tensor was convoluted by several filters until the layer of ζ to finally differentiate the actual and τηε counterfeit.

3) Learning Policy

The two-timescale update rule was applied to optimize the discriminator only once rather than many times, increasing time efficiency. The ADAM optimizer was applied with $\beta_1 = 0$, and $\beta_2 = 0.9$ for training. The training rate for the discriminator was set at 0.0003, and 0.0001 for the generator. This proposed AA-GAN was designed to create a 128×128×96 3D volume encoded in both the occupancy and orientation fields, utilizing 2D maps as input with a size of 1024×1024. The batch size for learning was set to 5. For the generator objective, the style and content weighting factors were set as: $\alpha = 1e-2$ and $\beta/\alpha = 5e+2$.

The selected layers for content loss were 0, 3, 6, and l=0,1,2,3,4 for style loss. If l=0, P(*X*) was eliminated from $L_{content}^{0}$ and L_{style}^{0}. Thus, by training the AA-GAN, more training images were generated and used to train the AB-MTEDeep classifier model. The trained classifier was applied to classify the test images into the mild, moderate, and severe AA classes.

IV. EXPERIMENTAL RESULTS

The effectiveness of the AA-GAN-AB-MTEDeep model was assessed and compared with the ones of existing models by implementing them in MATLAB 2017b using the Figaro1k and Dermnet databases. Of the images collected, 70% was used for training and the remaining 30% was used for testing. The considered existing models were the AB-MTEDeep [16], RICAP-CNN [17], EF-GAN-VGG16 [19], and IAGAN [22], which were applied to the Figaro1k and Dermnet databases for the AA classification, using the same proportions for the training and testing of the models. Figure 3 shows the generator and discriminator loss curves in the AA-GAN model, while Figure 4 depicts the training progress of the AA-GAN-AB-MTEDeep model for AA classification. Table II presents the confusion matrix for the AA-GAN-AB-MTEDeep model for testing, and Table III presents the performance results of the models for AA classification.

Figure 5 illustrates the accuracy values of various data augmentations with classification models on the Dermnet and Figaro1k databases. The accuracy of the AA-GAN-AB-

MTEDeep was 17.6% higher than RICAP-CNN's, 14% higher than the EF-GAN-VGG16's, 8.6% higher than the IAGAN's, and 1.9% higher than that of the AB-MTEDeep model. This is due to the augmentation of the number of training images to create an effective classification model.

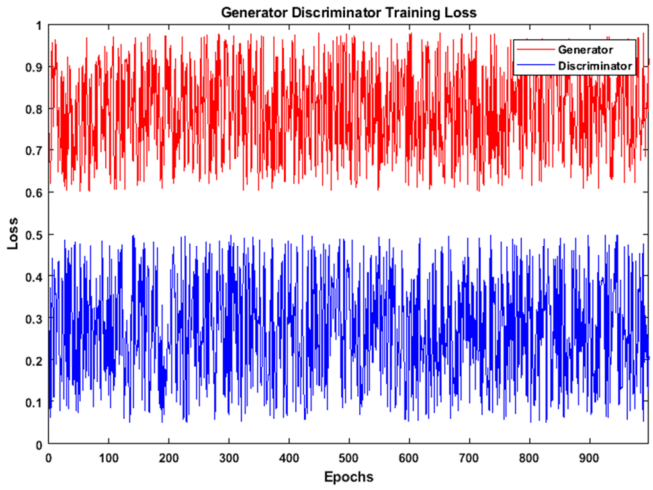

Fig. 3. Loss curve for generator and discriminator during training.

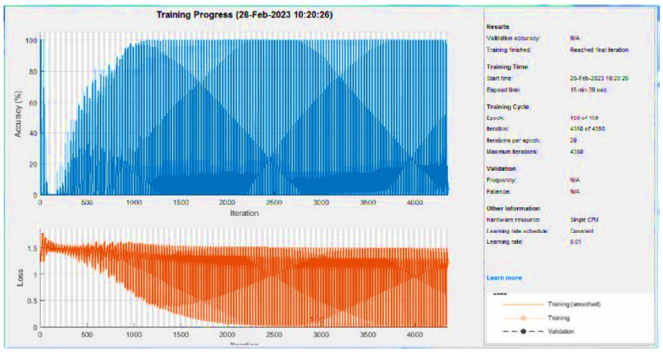

Fig. 4. Training progress of the AA-GAN-AB-MTEDeep model for AA classification (training accuracy curve and loss curve).

TABLE II. CONFUSION MATRIX OF THE AA-GAN-AB-MTEDEEP TESTING

		Classified			
	Classes	**0**	**1**	**2**	**3**
Actual	0	29	0	1	0
	1	0	7	0	0
	2	1	0	9	0
	3	0	0	0	9

TABLE III. PERFORMANCE ANALYSIS FOR THE AA CLASSIFICATION MODELS ON FIGARO1K AND DERMNET

Metrics	**RICAP -CNN**	**EF-GAN-VGG16**	**IAGAN**	**AB-MTEDeep**	**AA-GAN-AB-MTEDeep**
Precision (%)	81.48	84.05	88.19	94.06	95.8
Recall (%)	82.22	84.68	88.46	95.3	96.8
F-measure (%)	81.85	84.365	88.325	94.68	96.3
Accuracy (%)	82.31	84.86	89.22	95.11	96.94

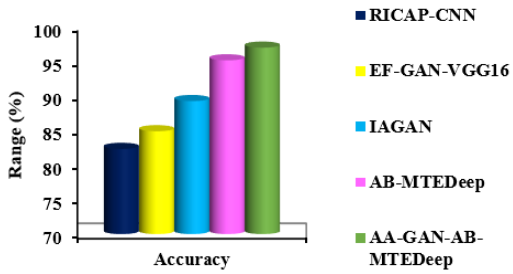

Fig. 5. Accuracy of AA-GAN-AB-MTEDeep and existing models.

V. CONCLUSION

This study presented the AA-GAN model designed to generate a large number of training images for AA classification. In this model, the structure and loss functions were similar to those of the standard GAN, which involves the generator and the discriminator network. The generator network was trained to create high-quality images based on the AA structure by retrieving the 2D orientation and confidence maps, along with the bust depth map from the original hair and scalp images. The discriminator was trained to distinguish original from synthetic images, which was given as feedback to the generator for minimizing its error. Furthermore, the generated synthetic images were used to train the AB-MTEDeep model for AA classification. The test results showed that the AA-GAN-AB-MTEDeep had a 96.94% accuracy, which was higher than the ones of the other variants of GAN with the AB-MTEDeep model to classify AA and scalp conditions. In the future, hybrid deep learning models with hyperparameter optimizers can be developed to improve AA classification performance.

REFERENCES

[1] K. York, N. Meah, B. Bhoyrul, and R. Sinclair, "A review of the treatment of male pattern hair loss," *Expert Opinion on Pharmacotherapy*, vol. 21, no. 5, pp. 603–612, Mar. 2020, https://doi.org/10.1080/14656566.2020.1721463.

[2] A. Ahmad, F. Khatoon, B. Khan, M. Mohsin, Lucknow, and A. Aligarh, "A Critical Review of Daus-Sadaf (Psoriasis): Unani & Modern Perspectives," *International Journal of Creative Research Thoughts*, vol. 8, no. 7, pp. 4570–4582, Jul. 2020, https://doi.org/10.13140/RG.2.2.25897.83040.

[3] D. I. Conde Hurtado, J. I. Vergara Rueda, J. L. Bermudez Florez, S. C. Cadena Infante, and A. J. Rodriguez Morales, "Potential Dermatological Conditions Resulting from a Prolonged Stay at Home during the COVID-19 Pandemic: A Review," *Acta dermatovenerologica Croatica: ADC*, vol. 29, no. 3, pp. 135–147, Dec. 2021.

[4] M. J. Adelman, L. M. Bedford, and G. A. Potts, "Clinical efficacy of popular oral hair growth supplement ingredients," *International Journal of Dermatology*, vol. 60, no. 10, pp. 1199–1210, Oct. 2021, https://doi.org/10.1111/ijd.15344.

[5] A. Egger, M. Tomic-Canic, and A. Tosti, "Advances in Stem Cell-Based Therapy for Hair Loss," *CellR4-- repair, replacement, regeneration, & reprogramming*, vol. 8, Sep. 2020, Art. no. e2894.

[6] F. Diotallevi, O. Simonetti, G. Rizzetto, E. Molinelli, G. Radi, and A. Offidani, "Biological Treatments for Pediatric Psoriasis: State of the Art and Future Perspectives," *International Journal of Molecular Sciences*, vol. 23, no. 19, Jan. 2022, Art. no. 11128, https://doi.org/10.3390/ijms231911128.

[7] L. C. Coates *et al.*, "Group for Research and Assessment of Psoriasis and Psoriatic Arthritis (GRAPPA): updated treatment recommendations for

psoriatic arthritis 2021," *Nature Reviews Rheumatology*, vol. 18, no. 8, pp. 465–479, Aug. 2022, https://doi.org/10.1038/s41584-022-00798-0.

[8] M. Sreenatha and P. B. Mallikarjuna, "A Fault Diagnosis Technique for Wind Turbine Gearbox: An Approach using Optimized BLSTM Neural Network with Undercomplete Autoencoder," *Engineering, Technology & Applied Science Research*, vol. 13, no. 1, pp. 10170–10174, Feb. 2023, https://doi.org/10.48084/etasr.5595.

[9] H. Reffad, A. Alti, and A. Almuhirat, "A Dynamic Adaptive Bio-Inspired Multi-Agent System for Healthcare Task Deployment," *Engineering, Technology & Applied Science Research*, vol. 13, no. 1, pp. 10192–10198, Feb. 2023, https://doi.org/10.48084/etasr.5570.

[10] V. C. Ho, T. H. Nguyen, T. Q. Nguyen, and D. D. Nguyen, "Application of Neural Networks for the Estimation of the Shear Strength of Circular RC Columns," *Engineering, Technology & Applied Science Research*, vol. 12, no. 6, pp. 9409–9413, Dec. 2022, https://doi.org/10.48084/etasr.5245.

[11] W.-J. Chang, L.-B. Chen, M.-C. Chen, Y.-C. Chiu, and J.-Y. Lin, "ScalpEye: A Deep Learning-Based Scalp Hair Inspection and Diagnosis System for Scalp Health," *IEEE Access*, vol. 8, pp. 134826–134837, 2020, https://doi.org/10.1109/ACCESS.2020.3010847.

[12] F. Zucchelli, N. Sharratt, K. Montgomery, and J. Chambers, "Men's experiences of alopecia areata: A qualitative study," *Health Psychology Open*, vol. 9, no. 2, Jul. 2022, Art. no. 205510292211215, https://doi.org/10.1177/20551029221121524.

[13] A. Alessandrini, F. Bruni, B. m. Piraccini, and M. Starace, "Common causes of hair loss – clinical manifestations, trichoscopy and therapy," *Journal of the European Academy of Dermatology and Venereology*, vol. 35, no. 3, pp. 629–640, 2021, https://doi.org/10.1111/jdv.17079.

[14] A. Elder, C. Ring, K. Heitmiller, Z. Gabriel, and N. Saedi, "The role of artificial intelligence in cosmetic dermatology—Current, upcoming, and future trends," *Journal of Cosmetic Dermatology*, vol. 20, no. 1, pp. 48–52, 2021, https://doi.org/10.1111/jocd.13797.

[15] C. Saraswathi, B. Pushpa, "Computer Imaging of Alopecia Areata and Scalp Detection: A Survey," *International Journal of Engineering Trends and Technology*, vol. 70, no. 8, pp. 347-358, 2022, https://doi.org/10.14445/22315381/IJETT-V70I8P236.

[16] C. Saraswathi and B. Pushpa, "Machine Learning Algorithm for Classification of Alopecia Areata from Human Scalp Hair Images," in *Computational Vision and Bio-Inspired Computing*, Singapore, 2023, pp. 269–288, https://doi.org/10.1007/978-981-19-9819-5_21.

[17] R. Takahashi, T. Matsubara, and K. Uehara, "Data Augmentation Using Random Image Cropping and Patching for Deep CNNs," *IEEE Transactions on Circuits and Systems for Video Technology*, vol. 30, no. 9, pp. 2917–2931, Sep. 2020, https://doi.org/10.1109/TCSVT.2019.2935128.

[18] Z. Qin, Z. Liu, P. Zhu, and Y. Xue, "A GAN-based image synthesis method for skin lesion classification," *Computer Methods and Programs in Biomedicine*, vol. 195, Oct. 2020, Art. no. 105568, https://doi.org/10.1016/j.cmpb.2020.105568.

[19] H. Xu *et al.*, "An Enhanced Framework of Generative Adversarial Networks (EF-GANs) for Environmental Microorganism Image Augmentation With Limited Rotation-Invariant Training Data," *IEEE Access*, vol. 8, pp. 187455–187469, 2020, https://doi.org/10.1109/ACCESS.2020.3031059.

[20] I. S. A. Abdelhalim, M. F. Mohamed, and Y. B. Mahdy, "Data augmentation for skin lesion using self-attention based progressive generative adversarial network," *Expert Systems with Applications*, vol. 165, p. 113922, Mar. 2021, https://doi.org/10.1016/j.eswa.2020.113922.

[21] K. Guo, T. Luo, M. Z. A. Bhuiyan, S. Ren, J. Zhang, and D. Zhou, "Zero shot augmentation learning in internet of biometric things for health signal processing," *Pattern Recognition Letters*, vol. 146, pp. 142–149, Jun. 2021, https://doi.org/10.1016/j.patrec.2021.03.012.

[22] S. Motamed, P. Rogalla, and F. Khalvati, "Data augmentation using Generative Adversarial Networks (GANs) for GAN-based detection of Pneumonia and COVID-19 in chest X-ray images," *Informatics in Medicine Unlocked*, vol. 27, Jan. 2021, Art. no. 100779, https://doi.org/10.1016/j.imu.2021.100779.

[23] C. Chen *et al.*, "Enhancing MR image segmentation with realistic adversarial data augmentation," *Medical Image Analysis*, vol. 82, Nov. 2022, Art. no. 102597, https://doi.org/10.1016/j.media.2022.102597.

[24] S. Nesteruk *et al.*, "XtremeAugment: Getting More From Your Data Through Combination of Image Collection and Image Augmentation," *IEEE Access*, vol. 10, pp. 24010–24028, 2022, https://doi.org/10.1109/ACCESS.2022.3154709.

[25] "Figaro 1K," *Figaro 1K | share Your Project.* http://projects.i-ctm.eu/it/progetto/figaro-1k.

[26] "DermNet skin disease atlas," *DermNet | Dermatology Resource*. https://dermnet.com.